Abstract

The use of elevated process pressures is described in the magnetron sputter deposition of titanium dioxide photocatalytic coatings to enable the direct low-temperature formation of the most photoactive titania crystal phase; anatase. Most other works on this subject deal with relatively low 'conventional' pressures (0.1 to 0.5 Pa). However, the present work describes pulsed DC reactive magnetron sputtering deposition of titanium dioxide thin films at process pressures in the range 2 – 5 Pa in a purpose-built sputtering rig. The influence of the other deposition conditions, such as pulse frequency and duty cycle, is also discussed. Additionally, a series of N-doped titania coatings was produced by using air as the reactive gas. The morphological and compositional properties of the coatings were studied using energy dispersive X-ray spectroscopy (EDX), scanning electron microscopy (SEM), X-ray diffraction (XRD), X-ray photoelectron spectroscopy (XPS) and atomic force microscopy (AFM). Wettability of the films was studied through measurement of water contact angles under UV light irradiation. Photocatalytic properties of the samples were assessed through the degradation of two model pollutants, methylene blue and stearic acid, under UV light irradiation. The results showed that elevated process pressures (4 Pa and above) allow the direct deposition of anatase titania films, without additional heat treatment, while amorphous titania tends to form at lower process pressures.

Keywords

Titanium dioxide; magnetron sputtering; pressure effect; N-doping; methylene blue; stearic acid

1. Introduction

Since its discovery in 1969 by Fujishima and Honda [1], photocatalytic titanium dioxide has been the subject of extensive research as a promising material for the degradation of organic pollutants and for water splitting processes [2-4]. Irradiation of titanium dioxide by light with energy equal or higher than its band gap value (3.2 eV for the anatase phase) results in the generation of electrons and holes. These photogenerated charge carriers are able to initiate photocatalytic processes where the holes oxidise donor molecules and the electrons reduce acceptor molecules. These processes lead, in turn, to the creation of highly reactive hydroxyl radicals able to oxidise organic pollutants in contact with the photocatalyst. Being an inexpensive, non-toxic and highly stable material, photocatalytic titanium dioxide finds applications in various fields, including self-cleaning surfaces, antimicrobial coatings, construction materials, etc. A wide variety of methods have been proposed to prolong the lifetime of photogenerated charge carriers and extend the photoresponse range of TiO_2, including photosensitization, generation of intrinsic defects, metal and non-metal doping [5-8], etc.

Of the different techniques used for the deposition of photocatalytic titania coatings (e.g. sol-gel, hydrothermal method, electron beam evaporation, etc.) magnetron sputtering (MS) is a method of particular industrial importance as it offers a number of advantages, including large area uniformity, good control over chemical and morphological properties and high reproducibility [9]. However, titanium dioxide coatings deposited by magnetron sputtering tend to be amorphous and require further thermal processing to develop crystallinity [7] (400 °C is typically referred as the anatase formation temperature), thus limiting the choice of substrates. Deposition of crystalline titania coatings often involves the use of radio frequency (RF) power supplies or the application of substrate bias, which in turn result in significant substrate heating and preclude the use of temperature-sensitive substrates, e.g. plastics. Recent developments in MS, such as high power impulse magnetron sputtering (HiPIMS), make possible the deposition of crystalline titania coatings without

additional thermal processing [10-12]. However, the power supplies are typically expensive and difficult to incorporate into a sputtering system and deposition rates are very low, compared to direct current (DC) sputtering. Therefore, pulsed DC (pDC) magnetron sputtering remains the process of choice for the deposition of photocatalytic coatings [13].

Since magnetron sputtering, in general, and its application for deposition of photocatalytic titania coatings, in particular, are relatively well-studied [9, 13], it is known that various process parameters can contribute to the properties of the deposited thin films, including process pressure, process gas ratios and target – substrate distance. Of the various sputtering parameters studied, process pressure changes are frequently reported to strongly influence the crystallinity and photocatalytic properties of the coatings [14-16]. For example, Pihosh, *et al*., showed that increasing the process pressure from 1.4 Pa to 2.3 Pa promoted the formation of anatase coatings, in preference to rutile or mixed phase coatings, with an associated improvement in photocatalytic activity [14]. Similarly, Šícha, *et al*., found a progressive shift from rutile to anatase and improvement in activity as the process pressure increased from 0.5 Pa to 2.0 Pa, which they illustrated in a phase zone model [17]. Rutile is the stable titania phase at higher temperatures and, therefore, a higher activation energy is required for its formation, compared to anatase. Consequently, the shift in crystalline phase from rutile to anatase has been attributed to the reduction in the energy delivered to the growing film, due to gas phase scattering in the plasma, as the process pressure is increased.

The present work describes deposition of crystalline photocatalytic titania coatings in a purpose-built magnetron sputtering rig. In contrast to the earlier reports on the effect of working pressure that typically deal with pressures in the range 1-2 Pa [17, 18] or below [19, 20], this study was performed at working pressures up to 5 Pa in order to study titania properties at higher deposition pressures and identify the optimum pressure for the deposition of crystalline photocatalytic TiO_2. This was followed by identification of pulse frequency and duty cycle effects on the structural and photocatalytic properties of the titania coatings. Once the optimum conditions were identified, the effect of nitrogen doping through the use of air as the reactive gas was studied, as nitrogen doping is frequently identified as an excellent method of extending the lifetime of photogenerated charge carriers and, therefore, improving the photocatalytic activity of titania thin films [21, 22].

2. Materials and methods

2.1. Deposition

Deposition of titanium dioxide coatings was performed as a single stage process in a purpose-built sputtering rig from one 7.5 cm diameter type II unbalanced planar magnetron. The schematic representation of the sputtering rig is given in Figure 1. The base pressure of 2×10^{-3} Pa, or below, was achieved by a combination of rotary (Leybold Trivac 16B) and turbomolecular (Leybold TurboVac i90) pumps. The magnetron was installed on the top of the chamber, facing the electrically floating substrate holder; the distance between the magnetron and substrate was kept as 5 cm for all deposition runs. A titanium target (99.99 % purity) was fitted to the magnetron. The deposition process was carried out in reactive mode in an argon / oxygen atmosphere for undoped TiO_2 coatings or an argon / dry air (N_2:O_2= 79:21 (vol.%)) atmosphere for N-doped TiO_2 coatings. The gas flow rates were controlled with mass-flow controllers, with the Ar flow rate fixed at 8sccm for all runs. The working pressure was varied from 1.5 to 5 Pa; variation of the working pressure was achieved without increasing the gas flow by adjusting the gate valve between the turbomolecular pump and the chamber. Power to the magnetron was delivered in pulsed DC (pDC) mode using an Advanced Energy Pinnacle Plus power supply. A power setting of 250 W was used for all deposition runs; pulse frequency and duty cycles were varied; an overview of deposition conditions used is given in the Table 1. To provide a better understanding of the effect of various deposition

parameters on the properties of the photocatalytic titania coatings, only one parameter was varied at a time. The coatings were deposited onto soda lime glass slides, which were ultrasonically pre-cleaned in propanol prior to deposition. The deposition time was 30 min for all the coatings studied. No additional substrate heating was provided and the deposition process temperature did not exceed 423 K (as identified using the temperature-sensitive crayons).

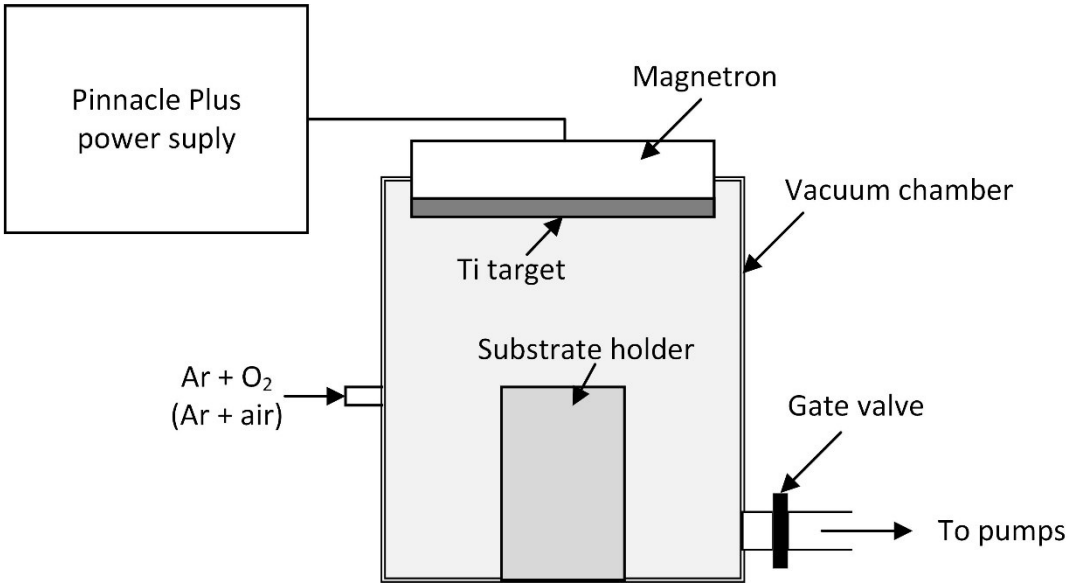

Figure 1. Schematic representation of the sputtering rig

2.2. Characterisation

The thickness of the coatings was measured with a stylus profilometry (Dektak™ surface profilometer) and verified by scanning electron microscopy (Zeiss Supra 40 VP-FEG-SEM) of fracture sections of the coatings. The composition of the coatings was investigated with energy-dispersive X-ray spectroscopy (EDX) (EDAX, Trident installed on a Zeiss Supra 40 VP-FEG-SEM). The microstructure and crystallinity of the thin films were analysed with Raman spectroscopy (Renishaw Invia, 514 nm laser) and X-ray diffraction (XRD) (Panalytical Xpert powder with CuKa1 radiation at 0.154 nm in grazing incidence mode at 1° over a scan range from 20° to 70° 2θ and the accelerating voltage and applied current were 40 kV and 30 mA, respectively). The oxidation state information was obtained by X-ray photoelectron spectroscopy (XPS) (AMICUS photoelectron spectrometer equipped with an MgKa X-ray as a primary excitation source, and using Ag 3d as a reference binding energy at 368.2 eV). Surface roughness and surface area values of the coatings were determined with atomic force microscopy (AFM) (Veeco NanoScope IV MultiMode AFM). The transmittance data of the coatings were obtained using an Ocean Optics USB4000 UV-visible spectrometer, which was used in turn to evaluate the band gap energy according to the Tauc plot method [23], by plotting $(\alpha h\nu)^{1/2}$ as a function of hν and extrapolating the linear region to the abscissa (where α is the absorbance coefficient, h is Plank's constant, ν is the frequency of vibration). The measurements of photoinduced wettability were preformed through analysis of water droplet contact angles (WCA) with a Theta Lite Optical tensiometer, while irradiating the samples with a UV light source (2 × 15 W 352 nm Sankyo Denki BLB lamps). Samples were kept in the dark for 24 h prior to the WCA measurements.

2.3. Photocatalytic activity assessment

Photocatalytic properties of the coatings were evaluated using methylene blue (MB) degradation and stearic acid (SA) degradation tests. Full descriptions of the tests are given elsewhere [24]. In

brief, for the MB degradation test, samples of the same geometrical size (1.5 x 2.5 cm^2) were immersed in 40 mL conditioning solution of methylene blue (concentration: 1.5 µmol/L) in the dark at room temperature for 30 min to reach an adsorption-desorption equilibrium. The samples were then withdrawn from the conditioning solution and immersed into 40 ml of testing solution (concentration: 1.5 µmol/L) with continuous magnetic stirring, while being irradiated with the same UV light source used for the wettability measurements (2 × 15 W 352 nm Sankyo Denki BLB lamps) for a total time of 1h. The concentration of the MB solution used was pre-defined experimentally to allow the detection of a photocatalytic response of each coating during a 1h experiment. Schematic representations of the setup and the emission spectrum of the UV light source used are given elsewhere [13, 25]; the integrated power flux to the coating was 4 mW/cm^2. According to the Lambert – Beer law, the concentration of the dye is proportional to the absorbance decay. The apparent first order rate constant, k_a, was used as a quantitative characterisation of the photocatalytic degradation rate of MB. Values of k_a were calculated from the gradient of the graph of $A_t/A_{t=0}$ versus time ($A_{t=0}$ and A_t are the absorbance values of methylene blue at the wavelength of 664 nm at time 0 and time of experiment, respectively). Reference tests were performed prior to the photocatalytic measurements, including blank substrates (soda lime glass and PET) under UV light and tests of each sample in the dark. As none of the reference tests showed more than 1% peak height decay in a 1h experiment, their effect was neglected in further calculations.

A stearic acid degradation test was used for verification of the MB test results. The detailed description of the test is given elsewhere [24]. In brief, samples of the same geometrical size (1.5 x 2.5 cm^2) were spin-coated with 0.1M stearic solution in acetone using an Osilla spin coater at 1000 rpm for 30 sec. After being spin-coated samples were kept in the dark for a total time of 1h to ensure full evaporation of the acetone from the surface of the samples. Monitoring of SA decomposition was performed every 24 h by Fourier transform infrared spectroscopy (FTIR) (Perkin Elmer Spectrum Two IR spectrometer) in the range 2700-3000 cm^{-1}. Infrared spectra were collected in absorbance mode; the amount of stearic acid on the surface of sample is proportional to the integrated area under the corresponding FTIR spectrum. The same light source as described earlier for the MB degradation tests was used for the SA degradation test; all samples were irradiated for 96 h in total.

3. Results and discussion

3.1. Coatings overview

A summary of deposition conditions, target current and voltage are given in the Table 1, as well as the visual appearance information. Visually all coatings produced using oxygen as the reactive gas were of similar appearance, optically transparent and uniform, with no visible signs of stresses or cracks. However, the coatings produced with using air as the reactive gas had different appearances, depending on the flow rate of the gas. Thus, sample Ti-A1 was of similar transparency characteristics as the Ti-O array, while coatings Ti-A2 – Ti-A4 were visually darker.

Table 1. Summary of deposition conditions and visual appearance for the studied coatings (Ar flow rate = 8sccm for all runs)

Sample ID	Working pressure, Pa	Frequency, kHz	Duty cycle, %	Reactive gas	Reactive gas flow, sccm	Target voltage, V	Target current, A	Coating visual appearance
Ti-O1	2.5	350	50	O_2	5.0	217	1.15	Colourless, transparent
Ti-O2	3.0	350	50	O_2	5.0	215	1.16	Colourless, transparent

Ti-O3	4.0	350	50	O_2	5.0	215	1.17	Colourless, transparent
Ti-O4	5.0	350	50	O_2	5.0	213	1.17	Colourless, transparent
Ti-O5	4.0	100	50	O_2	5.0	209	1.20	Colourless, transparent
Ti-O6	4.0	350	90	O_2	5.0	319	0.78	Colourless, transparent
Ti-O7	4.0	100	90	O_2	5.0	402	0.62	Colourless, transparent
Ti-A1	4.0	100	50	Air	5.0	230	1.08	Colourless, transparent
Ti-A2	4.0	100	50	Air	3.0	230	1.09	Light yellow, transparent
Ti-A3	4.0	100	50	Air	2.5	215	1.18	Brown, transparent
Ti-A4	4.0	100	50	Air	2.0	214	1.17	Dark brown, non-transparent

3.2. Compositional properties and thickness of the coatings (profilometry, EDX and SEM results)

As mentioned, the thickness of the coatings was measured with surface profilometry and verified with cross-sectional SEM (thickness measurements were conducted in triplicate, the mean data are presented in the Table 2). The thickness information is given in Table 2. It is obvious from the data presented that neither variation in pressure or pulse parameters had a significant effect on the coatings thickness. All samples deposited with oxygen as the reactive gas were ca. 100 nm thick. On the contrary, using air as the reactive gas had a considerable effect on the coatings thickness. Thus, the thickness of the samples from the Ti-A array decreased as the air flow increased at a constant argon flow rate. It was noted that the thickest coating, Ti-A4 deposited at an air flow of 2 sccm, was nearly 5 times thicker than the average thickness of the coatings deposited with O_2 only and was 3.5 times thicker than coating Ti-A1, deposited at an air flow rate of 5sccm. Since the process pressure and the argon flow rate were both kept constant, the effect of reducing the flow rate of air was to increase the proportion of argon, relative to nitrogen and oxygen, in the magnetron discharge. Consequently, the Ti target was maintained in a more metallic, less poisoned state, which is associated with higher deposition rates. An additional indication of a cleaner target surface is the reduction in target voltage observed as the air flow rate was reduced.

SEM images of selected samples are given in Figure 2. It can be seen that all films were uniform and densely packed, with relatively smooth surfaces. Samples deposited using air as the reactive gas had visibly larger grains, compared to those deposited in oxygen. No significant changes in the films microstructure as a response to variations in sputtering conditions could be seen from the cross-sectional SEM images of the samples.

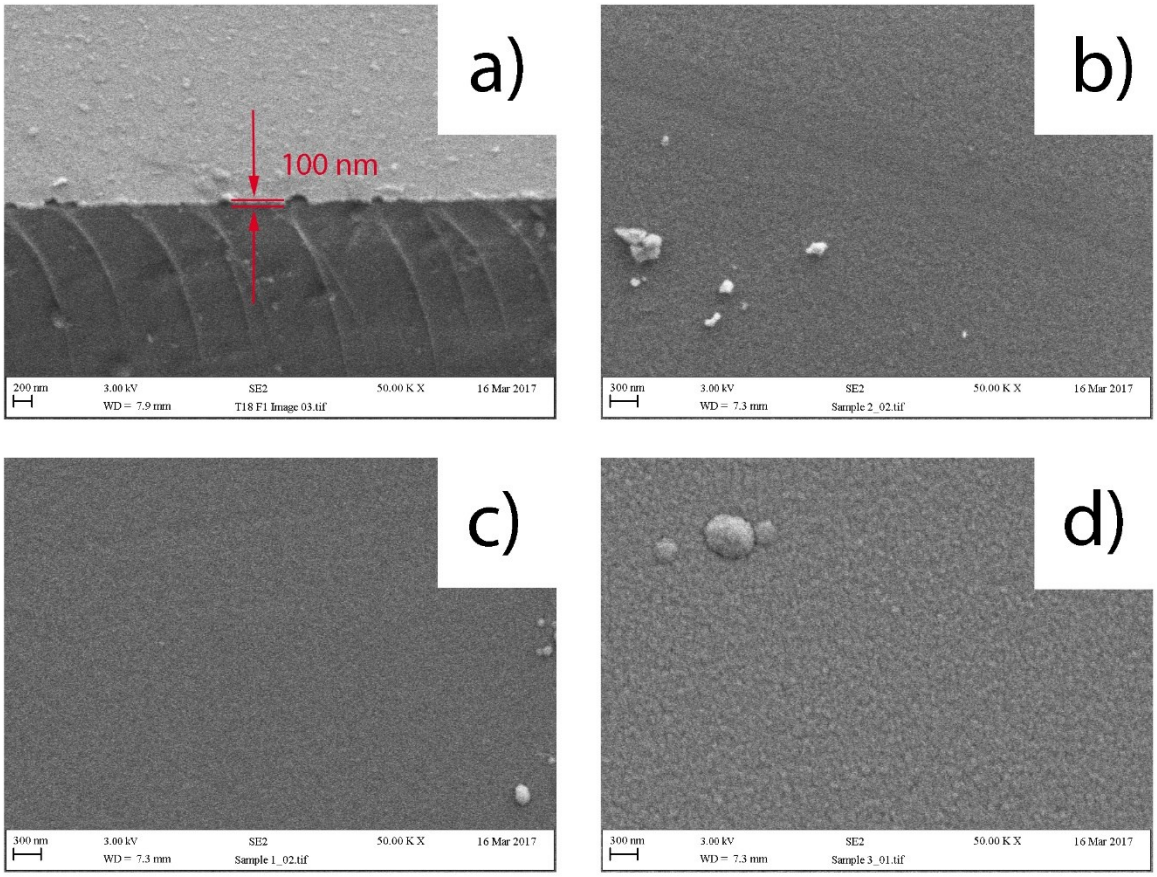

-

Figure 2. SEM images of selected coatings: a) SEM cross-sectional view of sample Ti-O5; SEM top view of sample Ti-O3; c) SEM top view of the sample Ti-O5; SEM top view of the sample Ti-A3

The compositional properties of the coatings, analysed with EDX, are given in the Table 2. It can be seen that the composition of the coatings deposited in oxygen only was close to stoichiometric TiO_2, with atomic ratios of titanium to oxygen of almost 1:2 in all cases. Variations of pressure and pulsing frequency / duty did not have a noticeable effect on Ti:O ratios. Use of air as the reactive gas resulted in the presence nitrogen in the coatings; the amount of nitrogen increased with the decrease of air flow – with the highest content of nitrogen for the sample Ti-A4 (ca. 28 at. %). Again, we attribute this to the degree of target poisoning being reduced as the air flow rate was reduced.

3.3. Crystallinity of the coatings (XRD)

Crystallinity of the coatings was assessed by means of X-ray diffraction (XRD). The XRD patterns of all studied samples are presented in Figure 3. It can clearly be seen that the samples deposited at lower pressures of 2.5 and 3 Pa (Ti-O1 and Ti-O2, respectively) were characterised with amorphous structures, since no peaks were observed on the XRD patterns of these coatings. However, as the pressure was increased further, evidence was observed of the presence in the coatings of the anatase phase, with characteristic peaks observed at 2θ angles of ca. 25.3°, 37.8°, 48.0°, 55.0° and 62.6° (crystallographic card number 96-900-8215). It should be noted that coatings deposited at 50% duty (Ti-O3 to TiO5) exhibited sharper and more pronounced anatase peaks, as compared to the samples deposited at 90% (Ti-O6 and TiO7). No peaks that could be attributed to the other titanium dioxide phases (e.g. rutile and brookite) were seen on the XRD patterns.

Of the coatings deposited with air as the reactive gas, the XRD pattern of sample Ti-A1 was very similar to that of sample Ti-O5 (reactively sputtered in oxygen under otherwise identical conditions). As the air flow was decreased, and therefore less oxygen was available for the reaction, the XRD patterns of the samples were distinctively different, with coating Ti-A2 being amorphous, while samples Ti-A3 and Ti-A4 exhibited peaks that could be attributed to the osbornite phase of titanium nitride (crystallographic card 96-101-1101) at 2θ angles of ca. 36.8°, 42.8° and 62.1°. Unsurprisingly, these peaks were more pronounced for the more nitrogen-rich sample Ti-A4.

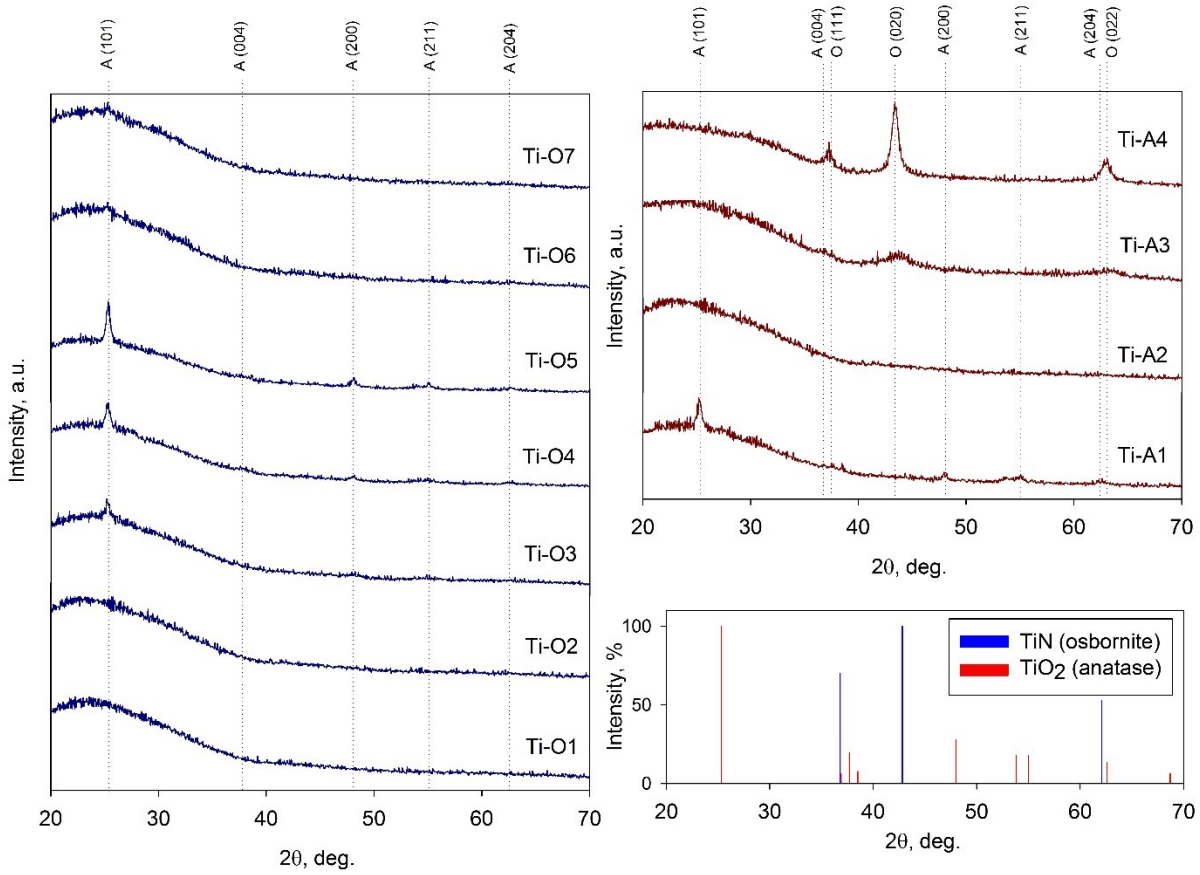

Figure 3. XRD diffraction patterns of the coatings: deposited using oxygen as reactive gas (left, blue); using air as reactive gas (top right, red); crystallographic patterns (bottom right)

3.4. Morphological properties of the films (AFM results)

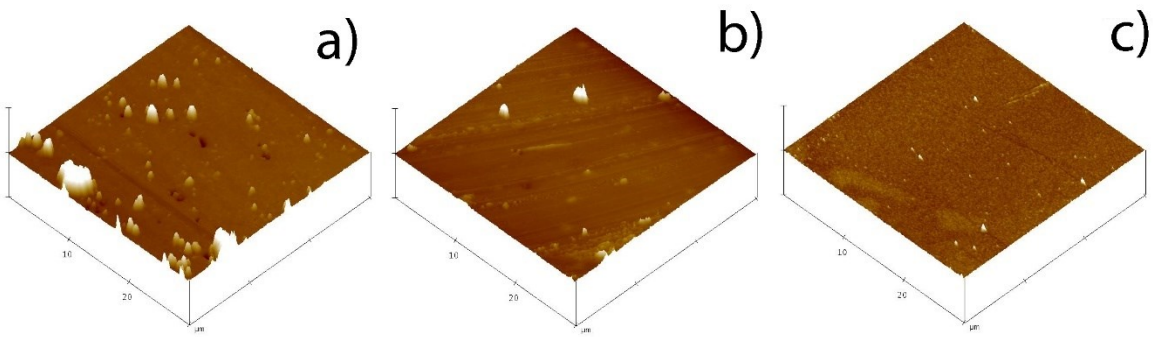

Figure 4. AFM results for selected samples deposited on glass substrate: a) Ti-O3; b) Ti-O5; c) Ti-A3

Morphological properties of the coatings were studied with atomic force microscopy (AFM); the values of the surface roughness and surface area are given in the Table 2. It can be seen that surface area values for all samples were ca. 900 μm^2, with variation below 1% between coatings deposited at different conditions. All coatings studied were relatively smooth and characterised with low surface roughness values. Examples of AFM images for selected coatings are given in Figure 4. It can be seen that undoped TiO_2 coatings (Figures 4a and 4b) were characterised with visibly smoother surface textures, but higher numbers of surface defects. On the contrary, nitrogen-rich coatings (Figure 4c) had coarser textures, but fewer surface defects, compared to undoped titania.

Table 2. Thickness information, compositional, morphological and optical properties of the coatings

Sample ID	Coating thickness, nm	Ti/O/N at.%	Crystal phase	Surface roughness, nm	Surface area, μm^2	Average visible transmittance, %	Band gap, eV
Ti-O1	85	34.6/65.4/0.0	amorphous	8.1	901.9	75.92	3.30
Ti-O2	90	34.9/65.1/0.0	amorphous	8.9	902.8	75.73	3.25
Ti-O3	105	34.1/65.9/0.0	TiO_2 anatase	5.1	900.9	76.09	3.24
Ti-O4	105	35.2/64.8/0.0	TiO_2 anatase	6.7	902.0	75.66	3.24
Ti-O5	100	34.4/65.6/0.0	TiO_2 anatase	7.8	903.5	75.82	3.21
Ti-O6	95	33.7/66.3/0.0	TiO_2 anatase	7.8	904.1	72.87	3.23
Ti-O7	90	34.8/62.2/0.0	TiO_2 anatase	6.0	905.3	76.56	3.22
Ti-A1	135	33.8/63.1/3.1	TiO_2 anatase	4.3	902.3	72.11	3.16
Ti-A2	185	30.3/61.2/8.5	amorphous	4.7	900.8	68.86	3.02
Ti-A3	415	31.9/48.0/20.1	TiN	2.1	900.8	49.04	2.11
Ti-A4	480	42.8/28.8/28.4	TiN	10.4	904.2	15.53	n/a

3.5. XPS results

Species and bonding states of the elements in the coatings were studied with X-ray photoelectron spectroscopy (XPS). Examples of the XPS results (sample Ti-O5) are given in Figure 5. The survey spectrum is given in Figure 5a; three strong peaks can be clearly seen on the spectrum. The presence of the C 1s peak at ca. 284 eV is typically explained with adventitious carbon contamination, while two peaks at 527 and 456 eV can be assigned to O 1s and Ti 2p excitations, respectively. High resolution spectra of Ti 2p and O 1s are given in figures 5b and 5c, respectively. The high resolution spectrum of the Ti 2p peak is deconvoluted into four peaks, where the peak positioned at 458.8 eV corresponds to Ti^{4+} $2p_{3/2}$, the peak at 464.6 eV can be assigned to Ti^{4+} $2p_{1/2}$ [24], and the peaks at 460.5 eV and 546.6 eV are typically assigned to Ti^{2+} $2p_{1/2}$ and Ti^{2+} $2p_{3/2}$, respectively [26]. Peaks in the high resolution spectrum of O 1s (figure 5c) are positioned at 530.2, 532.8 and 536.2 eV, and correspond to the T-O, C–O and C=O bonds, respectively. Identical peaks can be seen on the XPS spectra of all coatings deposited in oxygen as the reactive gas. For all of the coatings deposited in air as the reactive gas, a nitrogen 1s peak can be seen on the survey spectra at ca. 400 eV (not shown here). For coating Ti-A1, it can be deconvoluted into a single peak at 402.7 eV that can be assigned to substitutional nitrogen incorporated into the titanium dioxide lattice via O-Ti-N linkage [8]. As the

air flow reduced, the peak at 402.7 eV becomes dominated by a peak at 397.1 eV that can be assigned to the Ti-N bond.

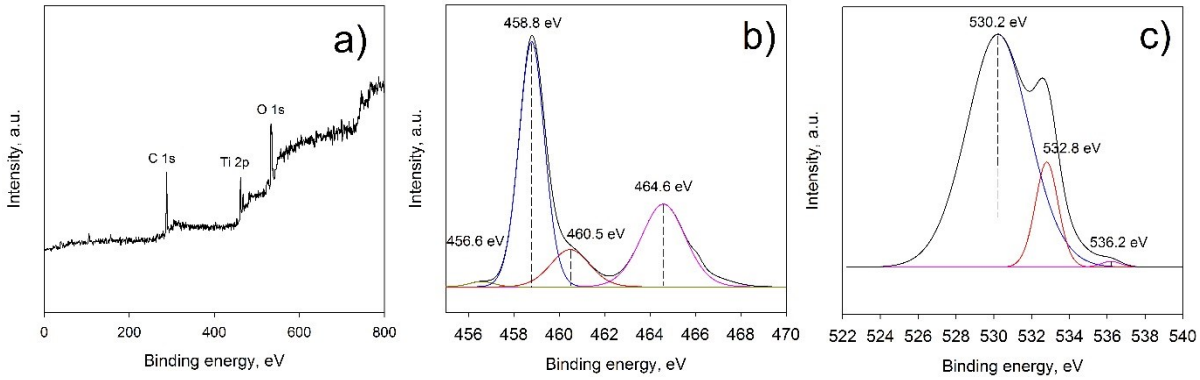

Figure 5. Example XPS results (sample Ti-O5): a) survey spectrum, b) Ti 2p spectrum; c) O 1s spectrum.

3.6. Optical properties and band gap calculation

Optical band gaps of the coatings were calculated using the Tauc plot method, as described in the Experimental section. Calculation examples for selected coatings (namely, Ti-O1, Ti-O3 and Ti-A1) are depicted in Figure 6. The calculated band gap values for all coatings studied in this work are given in Table 2.

The band gap (BG) values of the coatings deposited using oxygen as the reactive gas (undoped titania) are in good agreement with the literature information, where the BG for anatase titania is typically around 3.2 eV, and the BG of amorphous titania – around 3.4 eV [27]. As expected, some band gap narrowing can clearly be seen as a result of using air as a reactive gas. Thus, the band gap value of the sample Ti-A1 is 3.16 eV, and as the air flow decreased (less oxygen is available for reaction), further band gap narrowing was observed – with the lowest value calculated for the sample Ti-A3 (2.11 eV). It should be noted, that the band gap value for the sample Ti-A4 could not be calculated using the method above, as the optical transparency of the coating was too low. Judging from the band gap data observed, all of the photocatalytic coatings would be expected to be activated with the UV light source used in this work.

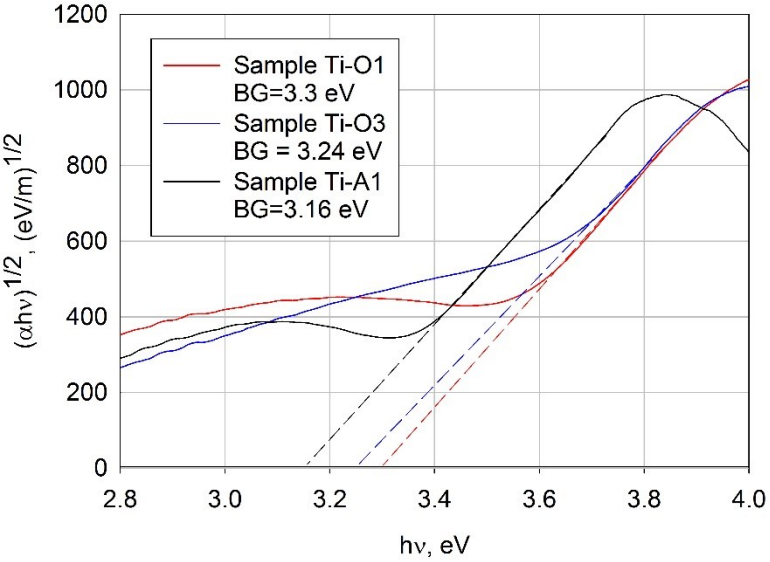

Figure 6. Examples of band gap calculation for selected titanium dioxide samples deposited onto glass substrate

3.7. Photoinduced wettability measurements

Changes in the wettability of the samples as a function of UV light irradiation were studied via deionised water contact angle (WCA) measurements. The values of WCA prior to UV irradiation (24h of dark storage) and after 1 h continuous UV irradiation are given in Table 3. Though the initial contact angles were quite different for all the samples, there are some trends that can be observed. Thus, samples deposited at lower process pressures were characterised with slightly higher values of CA (85 to 93 °), as compared to the samples deposited at higher pressures (64 to 71 °). It can be seen that all coatings deposited in oxygen (undoped TiO_2) demonstrated considerable reduction in WCA as a result of UV light irradiation (up to 63°). The films deposited at 90% duty cycle showed smaller reductions in WCA (~20°), compared to those deposited at 50% duty. As for the samples deposited in air, coatings Ti-A1 and Ti-A2 demonstrated similar behaviour to the Ti-O array, with reductions in CA after 1 h of UV light irradiation. However, no significant changes in WCA values were seen for the coatings Ti-A3 and Ti-A4 after irradiating them with the UV light.

It should be noted here, that despite the fact that the phenomenon of photoinduced hydrophilicity was observed for all studied coatings, except Ti-A3 and Ti-A4, none of the coatings demonstrated superhydrophilicity (WCA of 10° or lower) after 1 h irradiation.

Table 3. Results of wettability measurements and MB and SA photocatalytic decomposition test for titania coatings deposited onto glass substrate

Sample ID	Initial WCA, deg. (dark)	WCA after 1h UV irradiation, deg.	MB UV $k_a \times 10^{-5}$, s^{-1}	SA UV, $k_a \times 10^{-2}$, A cm^{-1} h^{-1}
Ti-O1	93	30	0.8	1.3
Ti-O2	85	59	1.2	1.7
Ti-O3	90	41	3.4	2.8
Ti-O4	71	63	1.1	1.2
Ti-O5	65	30	5.4	3.9
Ti-O6	64	41	3.0	1.9
Ti-O7	64	44	1.1	1.8

Ti-A1	62	32	4.7	3.4
Ti-A2	70	34	1.4	1.2
Ti-A3	105	95	0.7	0.8
Ti-A4	99	93	0.4	0.0

3.8. Photocatalytic test results

The photocatalytic properties of the coatings were assessed via two types of photocatalytic tests, namely, MB and SA decomposition under UV light irradiation.

The methylene blue decomposition reaction followed pseudo first order kinetics; the calculated values of the reaction constants are given in Table 3. MB decay rates vs experiment time of selected samples are shown in Figure 7a. It is evident that the highest MB degradation rates were seen for samples Ti-O5 and Ti-A1, while samples Ti-O3 and Ti-O6 exhibited lower, intermediate rates of dye degradation. Results for the rest of the undoped TiO_2 samples (namely Ti-O1, Ti-O2 Ti-O4 and Ti-O7) were very low and nitrogen-doped samples with high levels of N (Ti-A3 and Ti-A4) showed negligible rates of MB degradation.

Figure 7b presents selected results from the monitoring of stearic acid IR peaks under UV light illumination for a total time of 96 h. Quantitative characterisation of the degradation process is presented as reaction rate constants in Table 3 and graphically in Figure 7b. Control tests were performed with uncoated pieces of glass; no measurable peak reduction and consequently no stearic acid degradation was observed during 96 h of UV light irradiation, confirming the stability of SA under the chosen irradiation source. Similarly to the MB degradation test results, the highest degradation rates of SA were observed for samples Ti-O5 and Ti-A1. Sample Ti-O3 demonstrated moderate SA degradation ability, while the rest of the samples were characterised with considerably lower activity; no SA degradation was observed on the surface of the sample Ti-A4 during the 96 h hour experiment.

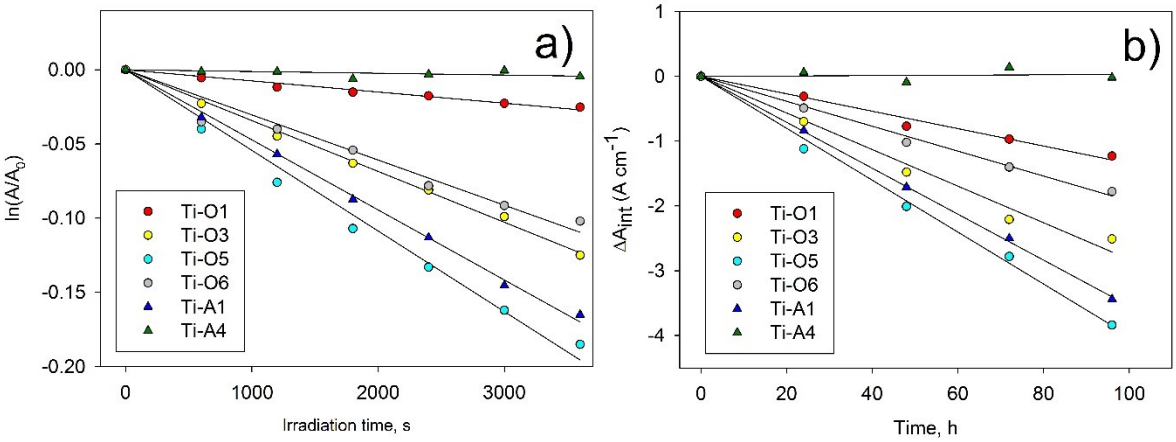

Figure 7. a) MB degradation kinetics in contact with selected samples under UV light; b) plots of the integrated area changes of the FTIR spectra of the stearic acid peaks (3000-2700 cm-1) under UV irradiation for selected samples

4. Discussion

It is well-established that, for low temperature magnetron sputter deposition processes, when the substrate cannot be heated, film structure and the presence of crystalline phases is mainly induced by the energy and flux of the particles incident at the substrate [9]. The work of Šícha, Musil and co-

workers concurs with this and indicates that, in the absence of significant substrate heating, the crystallisation of titania coatings depends on total pressure, partial pressure of oxygen, deposition rate and film thickness [28, 29], all of which influence the energy delivered to the growing film. Anatase is promoted by high total pressures and high oxygen partial pressures, which leads to target poisoning and low deposition rates. Operating at higher deposition rates in the transition mode at lower total and partial pressures suppresses anatase and leads to the formation of either rutile films or amorphous films, depending on the operating parameters and the film thickness.

Over the experimental conditions used in the present work, pressure also appears to be a major factor in determining crystal structure in titania films. Initial observations for the structure of the films deposited at the lower process pressures used here are in good agreement with the phase zone model for the formation of TiO_2 at temperatures below 180 °C developed by Šícha and co-workers [30]. According to this model, at process pressures of around 2 Pa (i.e. relatively high compared to most magnetron sputtering processes), titania films tend to have amorphous structures until they reach some value of minimum thickness; when the thickness is above this minimum value they form an anatase structure. However, the process pressures used in those experiments did not exceed 2 Pa, therefore no information on film growth at higher pressures was predicted by the model. The present work takes the deposition process to more elevated pressures and, as can be seen from the results, further increases in the process pressure result in the formation of anatase films, even though the deposition time was not increased and thickness of the films remained comparable to those deposited at lower pressures. Therefore, the results overall are in good agreement with the earlier work [30], which suggests that certain elevated process pressures would enable growth of very thin films (ca. 100 nm) with anatase structures and high photocatalytic activities. The absence of rutile peaks in the XRD patterns of the films can be explained with the fact that rutile is typically referred as a high temperature TiO_2 phase, and therefore it requires higher deposition energies compared to anatase. Based on the observed effects of pressure variation, a process pressure of 4 Pa was chosen as optimal for the investigation of further variation of the sputtering parameters.

Pulse frequency and duty cycle were the other parameters varied in the present work. Two pulse frequencies, namely 100 kHz and 350 kHz, at two values of duty cycles (50 and 90 %) were used for the deposition of TiO_2 films. It is generally known that, for mid-frequency pDC magnetron sputtering, film structure is again governed by the ion to atom ratio incident at the substrate. As shown in earlier works of Bradley *et al*. [31] and Kelly *et al*. [32], ion energy flux to the substrate increases with frequency and decreases with duty. Over the experimental conditions tested here, it appears that duty has the greater effect on coating structure. Coatings Ti-O4 and Ti-O5 were deposited at 350 and 100 kHz, respectively and 50% duty. Both formed anatase structures, although Ti-O5 showed stronger peaks and had noticeably higher photocatalytic activity. Coatings Ti-O6 and TiO7 were also deposited at 350 and 100 kHz, respectively but 90% duty. In these cases, the coatings were only very weakly crystalline (arguably amorphous), with low photocatalytic activity. Based on the deposition conditions tested here, it can be concluded that a combination of 4 Pa deposition pressure, 100 kHz pulse frequency and 50% duty cycle created the optimum flux for the deposition of anatase titanium dioxide coatings with good photocatalytic activity under UV irradiation. Therefore, the above conditions were selected for production of N-doped coatings through the use of air as the reactive gas.

It is a well-known fact that titanium preferentially reacts with oxygen, rather than with nitrogen. Using the same reactive gas flow of air as for the array of the coatings deposited in pure oxygen (5 sccm) produced a film with rather low N content (3.1 at.%). The assumption is that, at this flow rate,

there was still sufficient oxygen available to form a predominantly oxide film. Reduction of the reactive gas flow, whilst maintaining the same argon flow rate and total pressure, resulted in the N content increasing significantly (up to ca. 28 at.% in sample Ti-A4), as the relative amount of oxygen in the discharge decreased. However, doping of titanium dioxide with nitrogen reportedly leads to the distortion of titania crystal lattice, and consequently degradation in the films crystallinity [33]. Indeed, as can be seen on the XRD patterns, while sample Ti-A1 demonstrates anatase peaks, similar to Ti-O5 (deposited in oxygen under otherwise identical conditions), sample Ti-A2 is amorphous (and samples Ti-A3 and Ti-A4 are predominantly titanium nitride).

Even though increased deposition pressure is sometimes reported as a factor resulting in increasing the surface area [17], we did not observe noticeable changes of the surface area values. Variations of pulse frequency, duty cycle or doping with nitrogen did not affect the surface area values either. Therefore, the higher photocatalytic activity of these samples can be attributed here to their improved photocatalytic properties rather than higher area of contact with the pollutant.

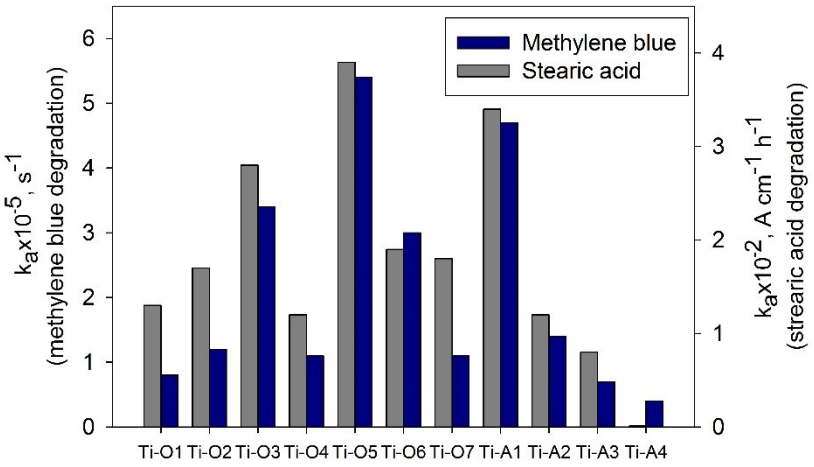

Figure 8. Bar chart of reaction constants for MB and SA degradation for undoped and N-doped titania coatings deposited onto glass substrate

The results of the two photocatalytic tests used revealed good correlation in the photocatalytic activity assessment of the samples. The results of both tests are summarised in the bar chart presented in the Figure 8. Additionally, the degradation data of the model pollutants are in good agreement with the XRD results of the samples crystallinity. As anatase is frequently reported as the most photoactive phase of titanium dioxide [34], not surprisingly the highest values of photocatalytic activity were observed for the samples with more pronounced anatase structures, compared to those exhibiting amorphous XRD patterns. The fact that very low / no photocatalytic activity was observed for samples Ti-A3 and Ti-A4 is in good agreement with the fact that titanium nitride was the predominant crystal phase in these coatings, and titanium nitride, unlike titanium dioxide, does not possess photocatalytic properties. Conversely, samples Ti-O5 and Ti-A1 showed rather high photocatalytic activity, however, the degradation rates of both SA and MB were slightly lower for the coating deposited in air. This can be explained with the fact that the nitrogen in our case was incorporated into the titania lattice in a substitutional manner, and, according to the literature, the presence of substitutional N does not necessarily result in the improvement of photocatalytic properties (as compared to interstitial nitrogen), as it causes faster recombination of the active photogenerated species [35].

Overall, the results of the present work are encouraging as they show that elevated process pressure, along with the optimised combination of other sputtering parameters, makes possible the deposition of thin crystalline titania films with high photocatalytic activity in a single stage process and without post-deposition thermal treatment. This finding is of high importance for the photocatalytic films industry, as it potentially enables the use of temperature-sensitive substrates, such as plastics. The follow up work will include further optimisation of the deposition parameters to maximise the photocatalytic activity, as well as deposition of optimised coatings onto polymeric substrates.

5. Conclusion

The present work discusses effects of elevated process pressure (2 Pa and above) on structural and photocatalytic properties of undoped and N-doped titanium dioxide thin films deposited by pDC reactive magnetron sputtering. Variation of the other sputtering parameters (pulse frequency and duty cycle) allowed preliminary optimisation of deposition condition in order to produce anatase titania. It was shown that anatase titania forms at process pressures of 4 Pa and above; increase of pulse frequency or duty cycle appeared to have a detrimental effect on anatase formation. The highest photocatalytic activity, based on degradation of model pollutants, namely methylene blue dye and stearic acid, was achieved for the coating deposited in an argon/oxygen atmosphere at 4 Pa working pressure, 100 kHz pulse frequency and 50% duty cycle. The above set of condition was selected for the production of N-doped titania films through use of air as the reactive gas; variation of nitrogen content in the coatings was achieved through reduction of the air flow at constant argon flow rate and total pressure, to create an oxygen deficiency. Despite the fact that nitrogen doping resulted in considerable band gap narrowing, no improvement of photocatalytic activity was observed, supposedly due to faster charge carrier recombination (low levels of N-doping) and formation of titanium nitride (high levels of N-doping). The data of photocatalytic efficacy for both photocatalytic tests used showed similar trends. Water contact angle measurements showed hydrophilicity development under UV light irradiation.

Overall, it can be concluded that the pDC reactive magnetron sputtering at elevated process pressures can be practical for the deposition of crystalline titania coatings without further thermal treatment, however precise optimisation of the other deposition conditions (e.g. pulsing parameters, reactive gas flow, etc.) is required to maximise the photocatalytic activity.

Acknowledgements

The authors wish to acknowledge the Royal Golden Jubilee Ph.D. scholarship from the Thailand Research Fund (PHD/0067/2554) for supporting the secondment of Rachan Klaysri at Manchester Metropolitan University, UK.

References

[1] H.K. Fujishima A., Kikuchi S., Photosensitized electrolytic oxidation on semiconducting n-type TiO_2 electrode, Kogyo Kagaku Zasshi 72 (1969) 108-113.
[2] M. Kitano, M. Matsuoka, M. Ueshima, M. Anpo, Recent developments in titanium oxide-based photocatalysts, Applied Catalysis A: General 325(1) (2007) 1-14.
[3] M. Pelaez, N.T. Nolan, S.C. Pillai, M.K. Seery, P. Falaras, A.G. Kontos, P.S.M. Dunlop, J.W.J. Hamilton, J.A. Byrne, K. O'Shea, M.H. Entezari, D.D. Dionysiou, A review on the visible light active titanium dioxide photocatalysts for environmental applications, Applied Catalysis B: Environmental 125(0) (2012) 331-349.
[4] A. Fujishima, X. Zhang, Titanium dioxide photocatalysis: present situation and future approaches, Comptes Rendus Chimie 9(5-6) (2006) 750-760.

[5] Y. Taga, Titanium oxide based visible light photocatalysts: Materials design and applications, Thin Solid Films 517(10) (2009) 3167-3172.
[6] S. Rehman, R. Ullah, A.M. Butt, N.D. Gohar, Strategies of making TiO_2 and ZnO visible light active, Journal of Hazardous Materials 170(2-3) (2009) 560-569.
[7] M. Ratova, P.J. Kelly, G.T. West, I. Iordanova, Enhanced properties of magnetron sputtered photocatalytic coatings via transition metal doping, Surface and Coatings Technology 228, Supplement 1(0) (2013) S544-S549.
[8] M. Ratova, G.T. West, P.J. Kelly, X. Xia, Y. Gao, Synergistic effect of doping with nitrogen and molybdenum on the photocatalytic properties of thin titania films, Vacuum 114(0) (2015) 205-212.
[9] P.J. Kelly, R.D. Arnell, Magnetron sputtering: a review of recent developments and applications, Vacuum 56(3) (2000) 159-172.
[10] M. Ratova, G.T. West, P.J. Kelly, Optimisation of HiPIMS photocatalytic titania coatings for low temperature deposition, Surface and Coatings Technology 250(0) (2014) 7-13.
[11] P.J. Kelly, P.M. Barker, S. Ostovarpour, M. Ratova, G.T. West, I. Iordanova, J.W. Bradley, Deposition of photocatalytic titania coatings on polymeric substrates by HiPIMS, Vacuum 86(12) (2012) 1880-1882.
[12] M. Ratova, G.T. West, P.J. Kelly, HiPIMS deposition of tungsten-doped titania coatings for photocatalytic applications, Vacuum 102(0) (2014) 48-50.
[13] P.J. Kelly, G.T. West, M. Ratova, L. Fisher, S. Ostovarpour, J. Verran, Structural Formation and Photocatalytic Activity of Magnetron Sputtered Titania and Doped-Titania Coatings, Molecules 19(10) (2014) 16327-16348.
[14] Y. Pihosh, M. Goto, A. Kasahara, M. Tosa, Photocatalytic property of TiO_2 thin films sputtered-deposited on unheated substrates, Applied Surface Science 256(4) (2009) 937-942.
[15] B. Liu, X. Zhao, Q. Zhao, C. Li, X. He, The effect of O_2 partial pressure on the structure and photocatalytic property of TiO_2 films prepared by sputtering, Materials Chemistry and Physics 90(1) (2005) 207-212.
[16] K. Eufinger, E.N. Janssen, H. Poelman, D. Poelman, R. De Gryse, G.B. Marin, The effect of argon pressure on the structural and photocatalytic characteristics of TiO_2 thin films deposited by d.c. magnetron sputtering, Thin Solid Films 515(2) (2006) 425-429.
[17] C. Zhang, W.Y. Ding, H.L. Wang, W.P. Chai, D.Y. Ju, Influences of working pressure on properties for TiO_2 films deposited by DC pulse magnetron sputtering, Journal of Environmental Sciences 21(6) (2009) 741-744.
[18] H. Fakhouri, J. Pulpytel, W. Smith, A. Zolfaghari, H.R. Mortaheb, F. Meshkini, R. Jafari, E. Sutter, F. Arefi-Khonsari, Control of the visible and UV light water splitting and photocatalysis of nitrogen doped TiO_2 thin films deposited by reactive magnetron sputtering, Applied Catalysis B: Environmental 144 (2014) 12-21.
[19] C.C. Hu, A.H. Chiou, C.T. Yang, W.J. Yang, J.Y. Kao, C.Y. Hsu, Best compromise for photocatalytic activity and hydrophilicity: N-doped TiO_2 films under UV light, Journal of Sol-Gel Science and Technology 81(1) (2017) 167-176.
[20] S.-H. Lee, E. Yamasue, H. Okumura, K.N. Ishihara, Effect of substrate roughness and working pressure on photocatalyst of N-doped TiOx films prepared by reactive sputtering with air, Applied Surface Science 324 (2015) 339-348.
[21] M.V. Dozzi, E. Selli, Doping TiO_2 with p-block elements: Effects on photocatalytic activity, Journal of Photochemistry and Photobiology C: Photochemistry Reviews 14(0) (2013) 13-28.
[22] R. Asahi, T. Morikawa, T. Ohwaki, K. Aoki, Y. Taga, Visible-Light Photocatalysis in Nitrogen-Doped Titanium Oxides, Science 293(5528) (2001) 269-271.
[23] J. Tauc, R. Grigorovici, A. Vancu, Optical Properties and Electronic Structure of Amorphous Germanium, physica status solidi (b) 15(2) (1966) 627-637.
[24] R. Klaysri, M. Ratova, P. Praserthdam, P. Kelly, Deposition of Visible Light-Active C-Doped Titania Films via Magnetron Sputtering Using CO_2 as a Source of Carbon, Nanomaterials 7(5) (2017) 113.

[25] M. Ratova, G. West, P. Kelly, Optimization Studies of Photocatalytic Tungsten-Doped Titania Coatings Deposited by Reactive Magnetron Co-Sputtering, Coatings 3(4) (2013) 194-207.
[26] V.V. Atuchin, V.G. Kesler, N.V. Pervukhina, Z. Zhang, Ti 2p and O 1s core levels and chemical bonding in titanium-bearing oxides, Journal of Electron Spectroscopy and Related Phenomena 152(1) (2006) 18-24.
[27] S. Valencia, J.M. Marín, G. Restrepo, Study of the Bandgap of Synthesized Titanium Dioxide Nanoparticules Using the Sol-Gel Method and a Hydrothermal Treatment, The Open Materials Science Journal 4 (2010) 5.
[28] J. Musil, D. Heřman, J. Šícha, Low-temperature sputtering of crystalline TiO_2 films, Journal of Vacuum Science & Technology A: Vacuum, Surfaces, and Films 24(3) (2006) 521-528.
[29] J. Šícha, D. Heřman, J. Musil, Z. Strýhal, J. Pavlík, Surface Morphology of Magnetron Sputtered TiO2 Films, Plasma Processes and Polymers 4(S1) (2007) S345-S349.
[30] J. Šícha, J. Musil, M. Meissner, R. Čerstvý, Nanostructure of photocatalytic TiO_2 films sputtered at temperatures below 200 °C, Applied Surface Science 254(13) (2008) 3793-3800.
[31] J.W. Bradley, H. Bäcker, Y. Aranda-Gonzalvo, P.J. Kelly, R.D. Arnell, The distribution of ion energies at the substrate in an asymmetric bi-polar pulsed DC magnetron discharge, Plasma Sources Science and Technology 11(2) (2002) 165.
[32] P.J. Kelly, A.A. Onifade, Y. Zhou, G.C.B. Clarke, M. Audronis, J.W. Bradley, The Influence of Pulse Frequency and Duty on the Deposition Rate in Pulsed Magnetron Sputtering, Plasma Processes and Polymers 4(3) (2007) 246-252.
[33] S. Peng, Y. Yang, G. Li, J.W. Jiang, K.W. Jin, T.T. Yao, K.X. Zhang, X. Cao, Y. Wang, G.B. Xu, Effect of N_2 flow rate on the properties of N doped TiO_2 films deposited by DC coupled RF magnetron sputtering, Journal of Alloys and Compounds 678 (2016) 355-359.
[34] P. Zeman, S. Takabayashi, Effect of total and oxygen partial pressures on structure of photocatalytic TiO_2 films sputtered on unheated substrate, Surface & Coatings Technology 153(1) (2002) 93-99.
[35] S.H. Lee, E. Yamasue, H. Okumura, K.N. Ishihara, Effect of oxygen and nitrogen concentration of nitrogen doped TiOx film as photocatalyst prepared by reactive sputtering, Applied Catalysis a-General 371(1-2) (2009) 179-190.